ACS OMEGA

http://pubs.acs.org/journal/acsodf

Article

Layered Manganese Dioxide Thin Films Intercalated with Ag^+ Ions Reduceable In Situ for Oxygen Reduction Reaction

Ryuichi Marukawa, Takayuki Kiso, Tomohito Shimizu, Yu Katayama, and Masaharu Nakayama*

Cite This: *ACS Omega* 2022, 7, 15854−15861

Read Online

ACCESS | Metrics & More | Article Recommendations | Supporting Information

ABSTRACT: The purpose of this study is to propose a new strategy based on electrodeposition to create binder-free composites of metallic silver supported on MnO_2. The process involves *in situ* reduction of the Ag^+ ions incorporated in the interlayer spaces of layered MnO_2 in an alkaline electrolyte without Ag^+ ions. The reduction process of the incorporated Ag^+ was monitored *in situ* based on the characteristic surface plasmon resonance in the visible region, and the resulting metallic Ag was identified by X-ray photoelectron spectroscopy. Because the formation of metallic Ag is only possible *via* electron injection into the Ag^+ ions between MnO_2 layers, the growth of Ag metals was inevitably limited, although the reduced Ag did not remain immobilized in the interlayers of MnO_2. The thus-formed Ag in the MnO_2 composite functioned as an electrocatalyst for the oxygen reduction reaction in a gas diffusion electrode system, showing a much better mass activity compared to Ag particles electrodeposited from an aqueous solution containing $AgNO_3$.

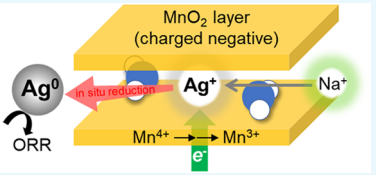

1. INTRODUCTION

Morphology control of catalyst particles is a common strategy for improving their activity. Catalysts with high activity have extremely high surface energies and thus require a suitable support to prevent their aggregation. In addition to carbonaceous materials, metal oxides can also serve as a support for catalysts. If the support can be prepared electrochemically, that is an added advantage because electrodeposition is essentially scalable and can yield thin uniform films, even on substrates with complex geometries, such as porous 3D scaffolds. In addition, no polymer binders or conducting additives are required, which makes it easier to determine the relationship between electrochemical performance and physicochemical properties of the active materials. We have reported that MnO_2 grown electrochemically serves not only as a catalyst but also as a support for immobilizing various catalytic ions.[1−3]

The oxygen reduction reaction (ORR) has been widely used in a variety of modern energy storage and conversion devices, such as fuel cells and metal−air batteries, where the slow ORR kinetics is a bottleneck for practical application. Pt- and Pt-containing alloys are considered to be the best cathode catalysts for both applications, but their cost and scarcity necessitates the search for cheaper alternatives. Silver-based catalysts have long been studied as alternatives to Pt materials due to their low cost, abundant availability, and relatively high stability for the ORR in alkaline solutions. In alkaline fuel cells, carbon-supported Ag has been widely and successfully used as the cathode catalyst.[4] However, the activity of Ag for the ORR is still unsatisfactory and needs improvement. On the other hand, MnO_2 has also been widely studied as one of the most promising candidates for the ORR in alkaline solution[5] because it is abundant in nature and inexpensive. Thus, the combination of Ag and MnO_2 at the nanoscale should be advantageous in the preparation of ORR catalysts.[6−14] For example, Liu et al. prepared a Ag−MnO_2/graphene composite by an immersion calcination method and found it to be as active as a state-of-the-art Pt/C catalyst in KOH solution.[6] Ag−Mn_3O_4/C has shown a higher electrocatalytic activity toward the ORR than a pure Ag catalyst.[7] Heating of Ag−MnO_2/C at 300 °C was also found to be effective.[8] Ag electrodeposited on reduced graphene oxide (GO)-supported MnO_2 exhibited promising ORR activity.[9] Shypunov et al. electrodeposited Ag onto a MnO_x/graphene composite and reported that the composite improved ORR activity relative to Ag/graphene, MnO_x/graphene, and bulk Ag.[10] However, neither of these electrodeposition methods imposed any limitations on the growth of Ag particles. Efficient Ag-based electrocatalysts remain in urgent demand in ORR applications. In view of future practical applications, we need as many options as possible for the production of catalysts. In addition, all of the above composite catalysts have been tested on a rotating disc electrode (RDE) immersed in an electrolytic solution, which may not reflect the performance of fuel cells composed of a gas diffusion electrode (GDE). Owing to the problem of low reactant mass transport, the reaction rates are quite different from those observed in actual fuel cell applications. This was very recently pointed out by Siegmund et al.,[15] where the authors described a noteworthy setup,

Received: February 17, 2022
Accepted: April 19, 2022
Published: April 28, 2022

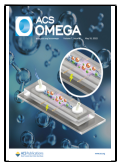

equipped with a GDE, more suitable for the evaluation of catalysts in fuel cells and metal−air batteries.[16]

We have introduced transition metals into the interlayers of layered MnO_2 and used them as catalysts for various reactions.[1−3,17] The transition metals exist as aqua-complexes isolated in the interlayers, unlike common heterogeneous catalysts such as transition-metal oxides and hydroxides. In this study, we intercalated Ag^+ ions into the interlayers of layered MnO_2 (birnessite) and reduced them to metallic Ag^0 species *in situ* by injecting electrons from an external circuit through the MnO_2 layers. The space enclosed by MnO_2 walls and a smaller number of precursor Ag^+ ions will inevitably limit the aggregation of cathodically generated Ag^0 species. The thus-obtained MnO_2-supported Ag catalysts fabricated on the GDE efficiently reduced gaseous oxygen, which was first demonstrated in the GDE half-cell setup (Figure S1) that was developed in ref 16.

2. RESULTS AND DISCUSSION

Figure 1 displays XRD patterns for MnO_2 thin films on FTO substrate in the as-deposited state (a) and after being immersed for 24 h in solutions with Ag^+ (b) and Na^+ (c). In the as-deposited state (a), diffraction peaks at 7.08°, 14.16°, and 21.25° in 2θ were observed. These equally spaced peaks can be attributed to the (001) plane of the layered MnO_2 intercalated with TBA^+ and second (002)- and third (003)-order diffractions, respectively.[18] The d-spacing of the 001 peak (d_{001}) is equivalent to the interlayer distance, which was calculated to be 1.26 nm using the Bragg formula. The d_{001} value obtained is in good agreement with the sum of the crystallographic thickness of a single MnO_2 sheet (~0.45 nm)[19] and the size of TBA^+ (0.81 nm in diameter).[20] Hereafter, the as-electrodeposited MnO_2 film with TBA^+ will be denoted as TBA^+/MnO_2. After immersing this film in the metal-containing solutions, the initial peaks in Figure 1a disappeared completely, and instead, new peaks appeared at higher angles, indicating smaller d-spacings.

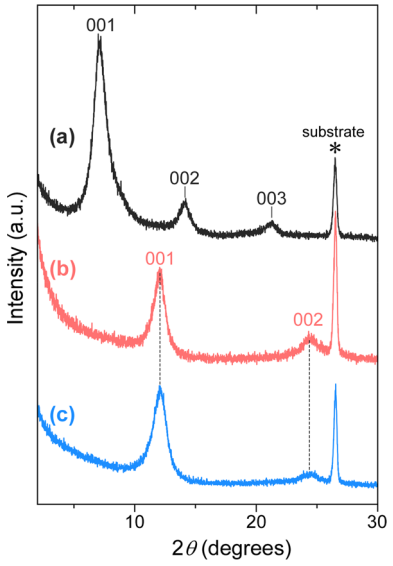

Figure 1. XRD patterns for a TBA^+/MnO_2 film (a) before and after immersion in (b) 5 mM $AgNO_3$ and (c) 2.5 mM Na_2SO_4 solutions.

In the film immersed in 5 mM $AgNO_3$ solution (Figure 1b), new peaks were detected at 12.2° and 24.6°. These peaks are typical of birnessite-type MnO_2 (PDF card no. 43-1456), whose interlayer distance was measured to be 0.73 nm. This structure accommodates a single layer of water molecules, together with cations (in this case Ag^+ ions) for compensating the negative charges on MnO_2 layers.[21] We verified that the same diffraction peaks were observed for the product similarly deposited on a CP substrate, as shown in Figure S2. After immersion in Na_2SO_4 solution, two peaks appeared in the same positions (12.2° and 24.5°). The decrease in interlayer spacing indicates the exchange of TBA^+, which has a large ionic radius and small charge density, with metal ions in the liquid phase. The water molecules, which are larger than Ag^+ and Na^+ ions, determine the interlayer distance of 0.73 nm (Figure S3a).

Figure 2 shows XPS spectra for FTO-supported MnO_2 thin films, in the as-deposited state (a) and after immersion for 24 h in solutions with Ag^+ (b) and Na^+ (c) ions. The energy separation between the doublet peaks in the Mn 3s region (ΔE(Mn 3s)) can be related to the oxidation state of Mn in the oxide. The ΔE(Mn 3s) value was calculated to be 4.6 eV for the as-deposited TBA^+/MnO_2, which is equivalent to an average oxidation state of 3.8 using the linear relationship (AOS = 9.67−1.27ΔE(Mn 3s)) reported in the literature.[22] Both the ΔE values after immersion in solutions with Ag^+ and Na^+ were estimated to be 4.6 eV, corresponding to an AOS of 3.8. Thus, there is no significant change in ΔE(3s) after immersion in metal-containing solutions, indicating that no electron transfer occurred between MnO_2 and the incorporated metals.

The N 1s signal appearing at 402.0 eV before immersion was attributed to cationic nitrogen, which verifies the inclusion of TBA^+.[23] This peak was lost after immersion in solutions of $AgNO_3$ and Na_2SO_4, and new peaks were detected in the Ag 3d and Na 1s regions, which were of course absent before immersion. The Ag 3d spectrum consists of two peaks at 367.8 and 373.8 eV, typical of Ag^+ ions.[24] In the Na 1s region, a peak due to Na^+ was observed at 1071 eV. The O 1s spectra of both the as-deposited TBA^+/MnO_2 and the films after immersion in metal solutions consist mainly of a contribution that is characteristic of lattice oxygen (M-O: 529.8−530.1 eV).[25] Small contributions at 532.3−532.6 eV, due to water molecules in the interlayer, were observed for the films after immersion. This suggests that the metal ions were coordinated with water molecules when incorporated into the interlayer spaces of birnessite MnO_2.[25] Combined with the XRD data in Figure 1, it is obvious that the TBA^+ ions between MnO_2 layers were replaced by the Na^+ and Ag^+ ions in solution through an ion-exchange mechanism. Hereafter, the MnO_2 films after being immersed in solutions with Ag^+ and Na^+ will be denoted as Ag^+/MnO_2 and Na^+/MnO_2.

Figure 3 shows CV measurement results for an FTO-supported Ag^+/MnO_2 film in an alkaline electrolyte, along with that for Na^+/MnO_2 for comparison. Na^+/MnO_2 showed a slight capacitive current without any distinct peaks. On the other hand, Ag^+/MnO_2 exhibited peaks at 1.07 and 1.32 V due to the redox of Ag^0/Ag^+ and peaks at 1.40 and 1.65 V for Ag^+/Ag^{2+}.[26] Since no Ag^+ ions were present in the solution, the observed redox peaks clearly indicate electron transfer between the incorporated Ag^+ ions and the underlying substrate through the MnO_2 layers.

XPS spectra were measured before and after polarizing the Ag^+/MnO_2 film at a cathodic potential of 1.0 V (vs RHE) for 2 h in the same electrolyte (1.0 M NaOH solution); the results

https://doi.org/10.1021/acsomega.2c00967
ACS Omega 2022, 7, 15854−15861

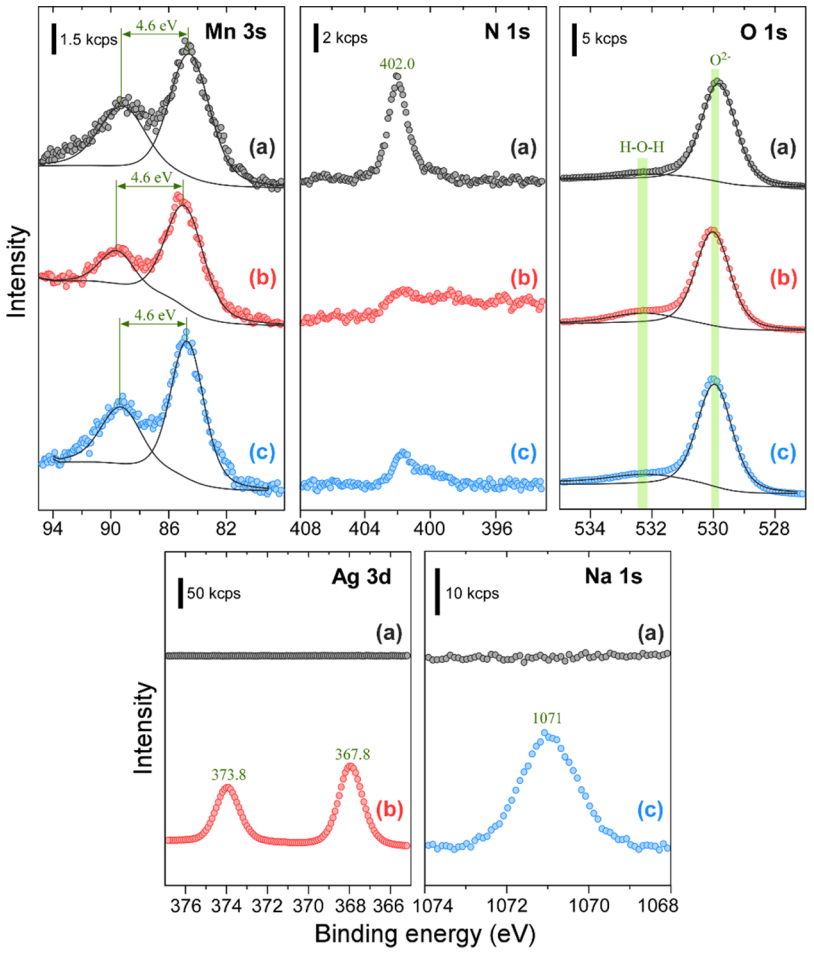

Figure 2. XPS spectra for TBA/MnO_2 (a) before and after immersion in solutions with (b) Ag^+ and (c) Na^+.

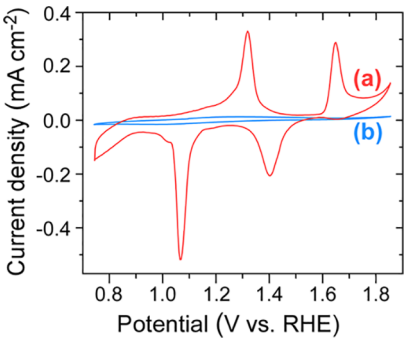

Figure 3. CV curves for (a) Ag^+/MnO_2 and (b) Na^+/MnO_2 films on an FTO substrate taken at a scan rate of 50 mV s^{-1} in 1.0 M NaOH solution after 10 cycles.

are displayed in Figure 4. As expected from the CV results in Figure 3a, the Ag^+ ions incorporated in the interlayer spaces of MnO_2 can be reduced, namely, Ag metal can be formed at 1.0 V. After polarization at 1.0 V, ΔE(Mn 3s) increased to 4.7 from 4.6 eV, corresponding to a decrease in Mn AOS from 3.8 to 3.7. The decreased AOS, relative to the as-deposited state, can be associated with the reduction of Mn^{4+} to Mn^{3+} in the oxide.

Note that the Ag 3d doublet peaks shifted to higher BE values, compared to before polarization. This can be ascribed to the emergence of Ag^0 species, along with a decrease in the cationic Ag^+ fraction. The residual Ag^+ might be the result of

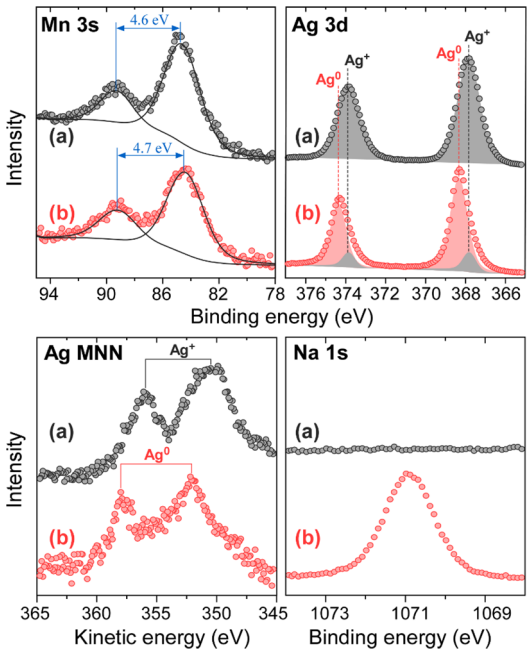

Figure 4. XPS spectra for Ag^+/MnO_2 obtained (a) before and (b) after a 2 h cathodic polarization run at 1.0 V (vs RHE) in 1.0 M NaOH solution.

https://doi.org/10.1021/acsomega.2c00967
ACS Omega 2022, 7, 15854−15861

air oxidation of the reduced Ag^0. The Auger parameter is considered more reliable than the BE of Ag 3d spectra for identifying the oxidation state of silver. In the figure, the spectra before and after polarization exhibited doublet peaks attributable to the Ag-MNN Auger structure transition, and the peaks shifted to higher BE upon polarization.[27] It is clear from the Ag 3d and Ag-MNN spectra that the Ag^+ ions were reduced *in situ* to metallic Ag in the interlayer space between MnO_2 layers. At the same time, a new peak due to Na^+ appeared in the Na 1s region.

On the basis of the results of the ICP-AES analysis, the atomic ratio of metals contained in the sample films was defined relative to the Mn content in the oxide. As shown in Table 1, the Ag/Mn ratio was estimated to be 0.20/1 in the Ag^+/MnO_2 film before polarization. This Ag/Mn ratio remained the same after polarization. Birnessite-type layered MnO_2 can be expressed by the general formula $C^+_xMnO_2 \cdot nH_2O$, where C^+ is a cation. The negative charges of MnO_2 sheets are electrically neutralized by the incorporation of guest cations (C^+). Considering the AOS of Mn determined by XPS and the Ag/Mn and Na/Mn determined by ICP-AES, the composition of the Ag-containing MnO_2 films before and after polarization can be expressed as $Ag^+_{0.20}Mn^{3+}_{0.2}Mn^{4+}_{0.8}O_2$ and $Ag^0_{0.20}Na^+_{0.37}Mn^{3+}_{0.3}Mn^{4+}_{0.7}O_2$, respectively. This result indicates that the decreases in the oxidation states of Ag and Mn upon reduction were compensated for by the incorporation of Na^+ ions from the electrolyte.

Table 1. AOS and Composition of Ag^+/MnO_2 Film before and after Cathodic Polarization at 1.0 V (vs RHE)

Ag^+/MnO_2	AOS(Mn) from XPS Mn 3s	Ag/Mn from ICP-AES	Na/Mn from ICP-AES
before	3.8	0.20	0.00
after	3.7	0.20	0.37

Figure 5 shows XRD patterns of an Ag^+/MnO_2 film obtained before and after cathodic polarization for 2 h in 1.0 M NaOH solution. After polarization, the positions of the 001 and 002 peaks shifted to slightly higher angles (lower d-spacings), while the layered structure itself remained upon the reduction of Ag^+/MnO_2. The shift in 001 is slight, but that in 002 is clearly visible because it doubles. This shift can be explained by an increase in electrostatic interaction between the reduced MnO_2 layers and the intercalated Na^+ ions, as shown in Figure S3b.

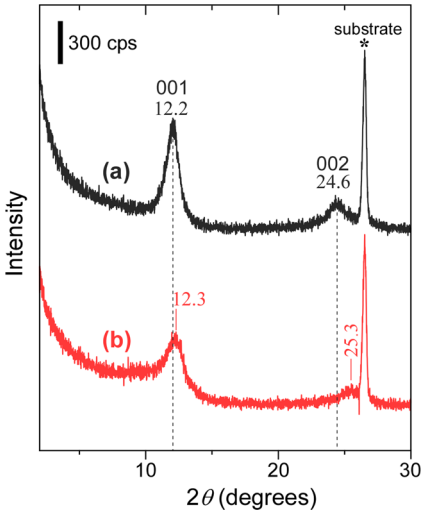

Figure 5. XRD patterns for Ag^+/MnO_2 film (a) before and (b) after cathodic polarization for 2 h in 1.0 M NaOH solution.

Moreover, the formation of metallic Ag in the interlayer spaces of MnO_2 was monitored *in situ* with a UV−vis spectrometer. Figure 6 shows the time course of UV−vis spectra of a Ag^+/MnO_2 film deposited on FTO, measured while a constant potential of 1.0 V (vs RHE) was applied in a NaOH electrolyte. The spectrum taken immediately after polarization was used as the base spectrum, while the UV−vis spectra after 3 min to 24 h are shown as difference spectra (Figure 6a). For comparison, the same measurement was conducted for Na^+/MnO_2 (Figure 6b). For Ag^+/MnO_2, the absorption that peaked at 400 nm increased with an increase in polarization time, which was absent in Figure 6b, increased with polarization time. The absorption peak at 400 nm can be attributed to the surface plasmon resonance of Ag nanoparticles.[28] This strongly suggests the formation of Ag nanoparticles as a result of cathodic reduction of Ag^+/MnO_2. However, we recognize that there is a seemingly broader increase in adsorption in the wavelength region above 500 nm. This is attributable not to absorption but to scattering by Ag particles that have grown large. Indeed, we examined the SEM images after polarization and found Ag particles with a relatively uniform size of several tens of nm to 100 nm that were reductively formed (Figure S4). The higher magnification image reveals that they are composed of even smaller particles, forming a raspberry-like morphology.

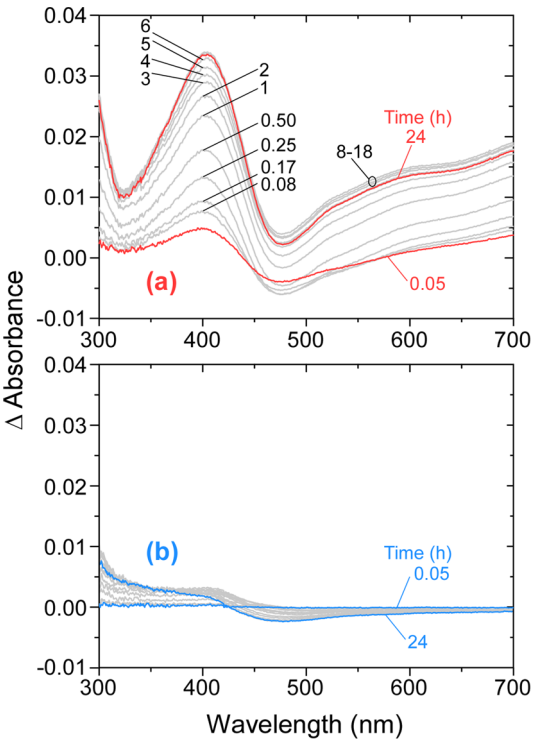

Figure 6. *In situ* UV−vis spectra for (a) Ag^+/MnO_2 and (b) Na^+/MnO_2 films on an FTO substrate during cathodic polarization for the noted times in 1.0 M NaOH solution.

ORR tests were performed using a GDE half-cell setup incorporating CP electrodes modified with catalysts. Figure 7 shows LSV curves for CP electrodes coated with Ag^+- and Na^+-intercalated MnO_2 films measured with 1.0 M NaOH solution

https://doi.org/10.1021/acsomega.2c00967
ACS Omega 2022, 7, 15854−15861

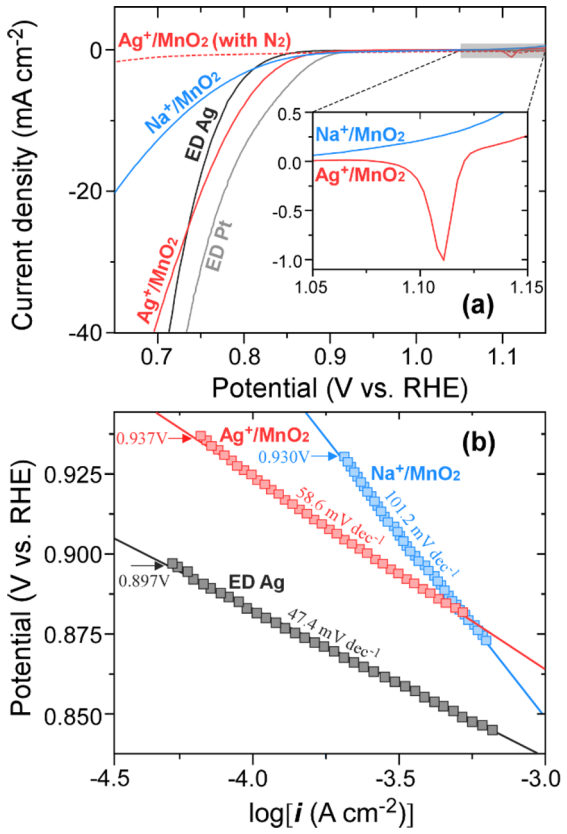

Figure 7. (a) LSV curves for Ag^+- and Na^+-intercalated MnO_2 films on a CP electrode measured in a solution of 1.0 M NaOH, along with those of electrodeposited Ag and Pt, and (b) the corresponding Tafel plots for Ag^+/MnO_2, Na^+/MnO_2, and electrodeposited Ag.

in the upper cell. Note that Ag^+/MnO_2 had not been subjected to cathodic polarization beforehand. During LSV measurements, O_2 gas was introduced from the bottom of the GDE cell. As shown in the inset, Ag^+/MnO_2 exhibited a peak at 1.11 V, which was attributed to the reduction of Ag^+ to Ag^0. The same cathodic peak was observed in Figure 3a. Naturally, this peak was not observed with Na^+/MnO_2, where another cathodic current due to the ORR started to appear at 0.9 V. Since this latter current was not observed under N_2 flow, it was attributed to the reduction of O_2 on the MnO_2 itself.[29] Note that the Ag^+/MnO_2 electrode provided an enhanced ORR current, compared to Na^+/MnO_2, which strongly suggests the catalytic effect of metallic Ag resulting from the *in situ* reduction of the intercalated Ag^+ ions between MnO_2 layers. The Tafel slope was estimated to be 101.2 and 58.6 mV dec^{-1} for the CP-supported Na^+/MnO_2 and Ag^+/MnO_2 films. The onset potential for the ORR was defined from the beginning of the linear region in the Tafel plot. The observed onset potential for Ag^+/MnO_2 (0.937 V) was slightly less negative compared to that for Na^+/MnO_2 (0.930 V). The Tafel slope for Ag^+/MnO_2 is close to that for ED Ag, and not to that for Na^+/MnO_2, suggesting the active site is the reductively formed Ag. We also conducted the same LSV measurement using a CP-supported Pt electrode, where the ORR current started to appear at the least negative potential.

The amount of the electrochemically active Ag in the Ag^+/MnO_2 film was determined on the basis of CV measurements obtained at 5 mV s^{-1} in 1.0 M NaOH electrolyte (Figure S5) and then compared with that of a Ag catalyst electrodeposited by the procedure reported in ref 30. Here, the amount of electrical charge delivered for the electrodeposition of the matrix materials, i.e., MnO_2 and Ag, was fixed at 200 mC cm^{-2}. Roughly the same redox peaks due to Ag^+/Ag^0 were observed at about 1.05 and 1.3 V. From the area underneath the reduction peak in Figure S5, the electrical charge delivered for the reduction of Ag^+ (Q_{red}) was calculated to be 0.78 and 7.49 mC $cm^{-2}_{\text{-geo}}$ for Ag^+/MnO_2 and electrodeposited Ag, respectively. Thus, the mass of electrochemically active Ag (Ag_{active} in g $cm^{-2}_{\text{-geo}}$) can be calculated by the equation

$$Ag_{active} = [Q_{red}/(n \times F)] \times M$$

where n is the number (= 1) of electrons transferred for the reduction of Ag^+, F is the Faraday constant (96,485 C mol^{-1}), and M is the molar mass of Ag (108.87 g mol^{-1}). As a result, Ag_{active} was calculated to be 8.81×10^{-7} and 8.46×10^{-6} g $cm^{-2}_{\text{-geo}}$ for Ag^+/MnO_2 and electrodeposited Ag, respectively. On the other hand, the total Ag amounts, determined on the basis of ICP-AES, were 1.75×10^{-6} and 2.00×10^{-5} g $cm^{-2}_{\text{-geo}}$ for Ag^+/MnO_2 and electrodeposited Ag metal, respectively.

The ORR responses of the two catalysts are compared in Figure 8, where each current density in Figure 7 is normalized

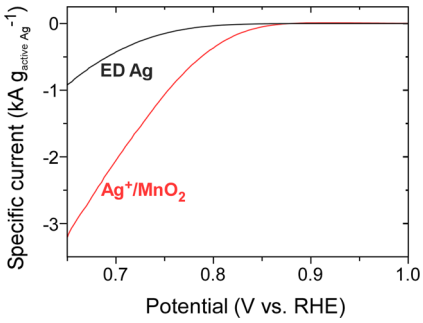

Figure 8. LSV curves for CP-supported (a) Ag^+/MnO_2 and (b) electrodeposited Ag in 1.0 M NaOH solution.

to the mass of Ag that was electrochemically active. As seen in Figure 7b, MnO_2 itself also possesses ORR activity, an dthe current density for Ag^+/MnO_2 was subtracted from that for Na^+/MnO_2. The figure also reveals that Ag particles supported in layered MnO_2 show a much superior ORR activity than electrodeposited Ag, indicating their enhanced mass activity toward the ORR. This can be ascribed to an increased utilization efficiency of the Ag^0 species generated as a result of *in situ* reduction of the Ag^+ ions accommodated in the interlayer spaces of layered MnO_2, compared to those electrodeposited from bulk Ag^+ solution.

3. CONCLUSION

The supported Ag fine particles were prepared by *in situ* reduction in alkaline electrolyte of the Ag^+ ions intercalated in the interlayer spaces of birnessite-type layered MnO_2. The generated Ag^0 species were not located between MnO_2 layers; however, their aggregation should be limited due to a small number of Ag^+ precursors and the small space enclosed by MnO_2 walls. The catalytic activity of the *in situ* reduced metal Ag toward the ORR was investigated in a GDE half-cell setup, which generated current densities of the order of several tens of mA cm^{-2}, much higher than the current density (several mA cm^{-2}) obtained using a rotating disk electrode immersed in an

https://doi.org/10.1021/acsomega.2c00967
ACS Omega 2022, 7, 15854−15861

electrolytic solution, due to the absence of mass transport limitation. The ORR activity of layered MnO_2 was significantly enhanced by Ag, not only due to an increase in the number of active sites, but also due to an increase in activity of the Ag itself, compared to pure Ag particles deposited.

4. EXPERIMENTAL SECTION

4.1. Materials. All chemicals were of reagent quality and used without further purification. $MnSO_4{\cdot}5H_2O$ (99.5%), Na_2SO_4 (99.0%), tetrabutylammonium chloride (TBA^+Cl^-, 99.5%), NH_4NO_3 (99.0%), NH_3 (28.0% in water), $KMnO_4$ (99.3%), NaOH (97.0%), $H_2PtCl_6{\cdot}6H_2O$ (98.5%), and H_2SO_4 (95.0%) were obtained from Wako Pure Chemicals. $AgNO_3$ (99.8%) was purchased from Ishizu Chemical, Ltd. All solutions were prepared with doubly distilled water and then deoxygenated by purging with purified nitrogen gas for more than 20 min immediately before each experiment.

4.2. Fabrication of Layered MnO_2 Intercalated with Ag^+ Ions. All electrochemical experiments were performed at room temperature in a standard three-electrode system attached to a potentiostat/galvanostat (SP-300, Bio-Logic Science Instruments). A platinum mesh (1.0 × 5.0 cm; thickness 0.5 mm; Nilaco) was used as the counter electrode, while Ag/AgCl (in saturated KCl) or Hg/HgO (in 1 M NaOH) was used as the reference electrode, depending on the pH of the electrolyte. A fluorine-doped tin oxide (FTO)-coated glass (thickness 1.8 mm; R = 10 Ω cm; Doujinsangyo Co., Ltd.) with a geometric area of 1.8 × 1.0 cm^2 was adopted as the working electrode to prepare films for structural characterization. In electrochemical tests, a sheet of carbon paper (CP; 1 cm^2, thickness 0.23 mm, GDL-39BB, Sigracet) was used owing to its large surface area, high electrical conductivity, and stability in alkaline media. Before electrodeposition, the FTO glass was degreased with acetone and then cleaned in an ultrasonic disperser with ethanol and water for 10 min each. Electrodeposition was made in an aqueous bath containing 2 mM $MnSO_4$ and 50 mM TBACl at room temperature. The working electrode was polarized at a constant potential of +1.0 V *vs* Ag/AgCl, while a fixed electrical charge of 20 or 200 mC cm^{-2} was delivered.[18] The thus-obtained film-coated electrode was immersed for 24 h in an aqueous solution of 5 mM $AgNO_3$ for replacing the initially incorporated bulkier TBA^+ ions by the denser Ag^+ ions. For comparison, the same procedure was conducted using a 2.5 mM Na_2SO_4 solution. The films deposited on FTO electrodes were rinsed with sufficient water and dried under vacuum in a desiccator prior to spectroscopic measurements.

Electrochemical tests were conducted by using a CP substrate as the working electrode. Two grams of $KMnO_4$ was slowly added to 20 mL of H_2SO_4, and a piece of CP was immersed in this solution for 2 min. After rinsing with water, the CP was maintained at 150 °C for 2 h in a muffle furnace and then rinsed with sufficient water. The CP was subsequently placed in a 3 mm diameter hole in the GDE cell (Figure S1) so that only the hydrophilic side was in contact with the bath for electrodeposition. The catalyst was prepared in the same way as on the FTO substrate. For comparison, Ag nanoparticles were electrodeposited on a CP substrate by applying a constant potential of −0.321 V *vs* Hg/HgO in a solution composed of 0.1 M $AgNO_3$, 0.5 M NH_4OH, and 0.1 M NH_4NO_3.[30] Similarly, Pt was electrodeposited on CP, where an aqueous solution of 0.02 M H_2PtCl_6 and 0.5 M H_2SO_4 was polarized at a constant current of −1 mA cm^{-2}.[31] In both cases, the charge delivered for electrodeposition here was also set to 200 mC cm^{-2}.

4.3. Structural Characterization. X-ray diffraction (XRD) patterns were collected on a diffractometer (Ultima IV, Rigaku) using Cu Kα radiation (λ = 0.154051 nm) as the source. Data were recorded over a 2θ region of 1°−50° at a scan speed of 1° min^{-1} with a beam current of 40 mA at a voltage of 40 kV. X-ray photoelectron spectra (XPS) were obtained using a Thermo Scientific K-Alpha spectrometer with a monochromatic Al Kα source (1486.6 eV). A pass energy of 50 eV and channel widths of 1.0 and 0.1 eV were adopted to collect wide- and narrow-range spectra, respectively. XPS fitting was made using CasaXPS software by setting the adventitious carbon peak to 284.8 eV. All spectra were deconvoluted using a Gaussian−Lorentzian line shape and a Shirley background. UV−vis spectra of the catalyst film on FTO immersed in a cell filled with 1 M NaOH solution were measured on a JASCO V-6700S, while the FTO electrode was polarized at the cathodic potential. Inductively coupled plasma-atomic emission spectroscopy (ICP-AES) was conducted using an SII Nano Technology SPS-3500. Samples were completely dissolved in 2 mL of HCl, to which HNO_3 was added to prepare an aqueous solution of 5.0 μM HNO_3.

4.4. Electrochemical Tests. Cyclic voltammetry (CV) was performed at 50 mV s^{-1} in a potential region of −0.2 to +0.9 V *vs* Hg/HgO in order to investigate the electrochemical properties of Ag^+/MnO_2 films on FTO electrodes. On the basis of the CV results, a constant potential was applied to reduce the Ag^+ ions between MnO_2 layers.

To clarify the catalytic activity for the ORR, linear sweep voltammetry (LSV) was performed in a GDE half-cell setup (Figure S1), which was the same as that reported in the literature.[16] A CP of 20 mm diameter was employed as the working electrode. The Ag/MnO_2 film was deposited on a spot with a diameter of 3 mm at the center of the top surface of the CP. The thus-fabricated CP electrode was placed on top of the stainless-steel body of the GDE half-cell. The upper cell body was made of poly(tetrafluoroethylene) and has a hole with a 3 mm diameter on the bottom to allow contact between the Ag^+/MnO_2 catalyst and the electrolyte. The upper cell compartment of the GDE setup was filled with a 1.0 M NaOH aqueous solution, and the carbon rod counter and Hg/HgO reference electrodes were inserted. O_2 gas was introduced from the bottom of the GDE cell at a flow speed of 40 mL min^{-1}, and after 30 min, LSV measurements were started while the O_2 flow continued. The solution resistance R_s was determined by electrochemical impedance spectroscopy (1 kHz, 10 mV amplified) and compensated. Thus, the potentials were reported with 85% *iR*-correction. All potentials were calibrated to the reversible hydrogen electrode (RHE); that is, E(RHE) = E(Hg/HgO) + 0.059 pH + 0.118.

■ ASSOCIATED CONTENT

Supporting Information

The Supporting Information is available free of charge at https://pubs.acs.org/doi/10.1021/acsomega.2c00967.

Scheme of GDE half-cell; XRD pattern of CP-supported Ag^+/MnO_2, expected structures of products; CVs of Ag^+/MnO_2 and ED Ag (PDF)

https://doi.org/10.1021/acsomega.2c00967
ACS Omega 2022, 7, 15854−15861

AUTHOR INFORMATION

Corresponding Author

Masaharu Nakayama − *Department of Applied Chemistry, Graduate School of Sciences and Technology for Innovation, Yamaguchi University, Ube 755-8611, Japan; Blue Energy Center for SGE Technology (BEST), Ube 755-8611, Japan;* orcid.org/0000-0002-5308-0126; Email: nkymm@yamaguchi-u.ac.jp

Authors

Ryuichi Marukawa − *Department of Applied Chemistry, Graduate School of Sciences and Technology for Innovation, Yamaguchi University, Ube 755-8611, Japan*

Takayuki Kiso − *Department of Applied Chemistry, Graduate School of Sciences and Technology for Innovation, Yamaguchi University, Ube 755-8611, Japan*

Tomohito Shimizu − *Department of Applied Chemistry, Graduate School of Sciences and Technology for Innovation, Yamaguchi University, Ube 755-8611, Japan*

Yu Katayama − *SANKEN (The Institute of Scientific and Industrial Research), Osaka University, Ibaraki 567-0047 Osaka, Japan;* orcid.org/0000-0002-7842-2938

Complete contact information is available at: https://pubs.acs.org/10.1021/acsomega.2c00967

Notes

The authors declare no competing financial interest.

ACKNOWLEDGMENTS

We gratefully acknowledge the financial support of the Japan Society for the Promotion of Science (Grant No. 20H02844).

REFERENCES

(1) Nagita, K.; Yuhara, Y.; Fujii, K.; Katayama, Y.; Nakayama, M. Ni- and Cu-co-Intercalated Layered Manganese Oxide for Highly Efficient Electro-Oxidation of Ammonia Selective to Nitrogen. *ACS Appl. Mater. Interfaces* **2021**, *13*, 28098−28107.

(2) Nakayama, M.; Suzuki, K.; Fujii, K. Single-ion catalyst of Ni^{2+} anchored in the interlayer space of layered MnO_2 for electro-oxidation of ethanol in alkaline electrolyte. *Electrochem. Commun.* **2019**, *105*, 106492.

(3) Fujimoto, K.; Okada, T.; Nakayama, M. Enhanced Oxygen Evolution Reaction Activity of Co Ions Isolated in the Interlayer Space of Buserite MnO_2. *J. Phys. Chem. C* **2018**, *122*, 8406−8413.

(4) Gülzow, E.; Wagner, N.; Schulze, M. Preparation of Gas Diffusion Electrodes with Silver Catalysts for Alkaline Fuel Cells. *Fuel Cells* **2003**, *3*, 67−72.

(5) Roche, I.; Chaînet, E.; Chatenet, M.; Vondrák, J. Carbon Supported Manganese Oxide Nanoparticles as Electrocatalysts for the Oxygen Reduction Reaction (ORR) in Alkaline Medium: Physical Characterizations and ORR Mechanism. *J. Phys. Chem. C* **2007**, *111*, 1434−1443.

(6) Liu, S.; Qin, X. Preparation of a Ag-MnO_2/graphene composite for the oxygen reduction reaction in alkaline solution. *RSC Adv.* **2015**, *5*, 15627−15633.

(7) Liu, J.; Liu, J.; Song, W.; Wang, F.; Song, Y. The role of electronic interaction in the use of Ag and Mn_3O_4 hybrid nanocrystals covalently coupled with carbon as advanced oxygen reduction electrocatalysts. *J. Mater. Chem. A* **2014**, *2*, 17477−17488.

(8) Wu, Q.; Jiang, L.; Qi, L.; Yuan, L.; Wang, E.; Sun, G. Electrocatalytic activity and stability of Ag-MnOx/C composites toward oxygen reduction reaction in alkaline solution. *Electrochim. Acta* **2014**, *123*, 167−175.

(9) Lee, K.; Ahmed, M. S.; Jeon, S. Electrochemical deposition of silver on manganese dioxide coated reduced graphene oxide for enhanced oxygen reduction reaction. *J. Power Sources* **2015**, *288*, 261−269.

(10) Shypunov, I.; Kongi, N.; Kozlova, J.; Matisen, L.; Ritslaid, P.; Sammelselg, V.; Tammeveski, K. Enhanced Oxygen Reduction Reaction Activity with Electrodeposited Ag on Manganese Oxide-Graphene Supported Electrocatalyst. *Electrocatalysis* **2015**, *6*, 465−471.

(11) Park, S.-A.; Lim, H.; Kim, Y.-T. Enhanced Oxygen Reduction Reaction Activity Due to Electronic Effects between Ag and Mn_3O_4 in Alkaline Media. *ACS Catal.* **2015**, *5*, 3995−4002.

(12) Sun, S.; Miao, H.; Xue, Y.; Wang, Q.; Li, S.; Liu, Z. Oxygen reduction reaction catalysts of manganese oxide decorated by silver nanoparticles for aluminum-air batteries. *Electrochim. Acta* **2016**, *214*, 49−55.

(13) Sun, S.; Miao, H.; Xue, Y.; Wang, Q.; Zhang, Q.; Dong, Z.; Li, S.; Huang, H.; Liu, Z. High Electrocatalytic Activity of Silver-Doped Manganese Dioxide toward Oxygen Reduction Reaction in Aluminum-Air Battery. *J. Electrochem. Soc.* **2017**, *164*, F768.

(14) Wang, W.; Chen, J.-Q.; Tao, Y.-R.; Zhu, S.-N.; Zhang, Y.-X.; Wu, X.-C. Flowerlike Ag-Supported Ce-Doped Mn_3O_4 Nanosheet Heterostructure for a Highly Efficient Oxygen Reduction Reaction: Roles of Metal Oxides in Ag Surface States. *ACS Catal.* **2019**, *9*, 3498−3510.

(15) Siegmund, D.; Metz, S.; Peinecke, V.; Warner, T. E.; Cremers, C.; Grevé, A.; Smolinka, T.; Segets, D.; Apfel, U.-P. Crossing the Valley of Death: From Fundamental to Applied Research in Electrolysis. *JACS Au* **2021**, *1*, 527−535.

(16) Inaba, M.; Jensen, A. W.; Sievers, G. W.; Escudero-Escribano, M.; Zana, A.; Arenz, M. Benchmarking high surface area electrocatalysts in a gas diffusion electrode: Measurement of oxygen reduction activities under realistic conditions. *Energy Environ. Sci.* **2018**, *11*, 988−994.

(17) Nakayama, M.; Fujimoto, K.; Kobayakawa, T.; Okada, T. A binder-free thin film anode composed of Co^{2+}-intercalated buserite grown on carbon cloth for oxygen evolution reaction. *Electrochem. Commun.* **2017**, *84*, 24−27.

(18) Nakayama, M.; Konishi, S.; Tagashira, H.; Ogura, K. Electrochemical synthesis of layered manganese oxides intercalated with tetraalkylammonium ions. *Langmuir* **2005**, *21*, 354−359.

(19) Post, J. E.; Veblen, D. R. Crystal structure determinations of synthetic sodium, and potassium birnessite using TEM and the Rietveld method. *Am. Mineral.* **1990**, *75*, 477−489.

(20) Criss, C. M.; Mastroianni, M. J. Some observations on the viscosity coefficients of ions in various solvents. *J. Phys. Chem.* **1971**, *75*, 2532−2534.

(21) Tian, Z.-R.; Xia, G.; Luo, J.; Suib, S. L.; Navrotsky, A. Effects of Water, Cations, and Structure on Energetics of Layer and Framework Phases, $Na_xMg_yMnO_2{\cdot}nH_2O$. *J. Phys. Chem. B* **2000**, *104*, 5035−5039.

(22) Beyreuther, E.; Grafström, S.; Eng, L. M.; Thiele, C.; Dörr, K. XPS investigation of Mn valence in lanthanum Manganite thin films under variation of oxygen content. *Phys. Rev. B* **2006**, *73*, 155425.

(23) Yang, D. Q.; Rochette, J. F.; Sacher, E. Spectroscopic evidence for pi-pi interaction between poly(diallyl dimethylammonium) chloride and multiwalled carbon nanotubes. *J. Phys. Chem. B* **2005**, *109*, 4481−4484.

(24) Lützenkirchen-Hecht, D.; Strehblow, H.-H. Anodic silver (II) oxides investigated by combined electrochemistry, ex situ XPS and in situ X-ray absorption spectroscopy. *Surf. Interface Anal.* **2009**, *41*, 820−829.

(25) Chigane, M.; Ishikawa, M. Manganese Oxide Thin Film Preparation by Potentiostatic Electrolyses and Electrochromism. *J. Electrochem. Soc.* **2000**, *147*, 2246−2251.

(26) Mikhlin, Y. L.; Vishnyakova, E. A.; Romanchenko, A. S.; Saikova, S. V.; Likhatski, M. N.; Larichev, Y. V.; Tuzikov, F. V.; Zaikovskii, V. I.; Zharkov, S. M. Oxidation of Ag nanoparticles in aqueous media: Effect of particle size and capping. *Appl. Surf. Sci.* **2014**, *297*, 75−83.

(27) Ferraria, A. M.; Carapeto, A. P.; Botelho do Rego, A. M. X-ray photoelectron spectroscopy: Silver salts revisited. *Vacuum* **2012**, *86*, 1988−1991.
(28) Van Hyning, D. L.; Zukoski, C. F. Formation Mechanisms and Aggregation Behavior of Borohydride Reduced Silver Particles. *Langmuir* **1998**, *14*, 7034−7046.
(29) Meng, Y.; Song, W.; Huang, H.; Ren, Z.; Chen, S.-y.; Suib, S. L. Structure-Property Relationship of Bifunctional MnO_2 Nanostructures: Highly Efficient, Ultra-Stable Electrochemical Water Oxidation and Oxygen Reduction Reaction Catalysts Identified in Alkaline Media. *J. Am. Chem. Soc.* **2014**, *136*, 11452−11464.
(30) de Oliveira, G. M.; Barbosa, L. L.; Broggi, R. L.; Carlos, I. A. Voltammetric study of the influence of EDTA on the silver electrodeposition and morphological and structural characterization of silver films. *J. Electroanal. Chem.* **2005**, *578*, 151−158.
(31) Lertviriyapaisan, S.; Tantavichet, N. Sublayers for Pt catalyst electrodeposition electrodes in PEMFC. *Int. J. Hydrogen Energy* **2010**, *35*, 10464−10471.

https://doi.org/10.1021/acsomega.2c00967
ACS Omega 2022, 7, 15854−15861